

Design of Commonly-Resonated Extended Interaction Circuits for Submillimeter-Wave Phase-Locked Oscillators

Bi Liangjie, Li Hailong, Wang Bin, Meng Lin, Yin Yong

(School of Electronic Science and Engineering, University of Electronic Science and Technology of China, No. 2006, Xiyuan Ave, West Hi-Tech Zone, Chengdu 611731, China)

Abstract: In this paper, a scheme of commonly-resonated extended interaction circuit system based on high order TM_{n1} mode is proposed to lock the phases of two extended interaction oscillators (EIOs) for generating high power at G-band. Two separate EIOs are coupled through a specific single-gap coupling field supported by a designed gap waveguide with length (L_g), which form the phase-locked EIOs based on the commonly-resonated system. As a whole system, the system has been focused on with mode analysis based on different single-gap coupling field, mode hopping, which presents the variation of phase difference between the two-beam-wave interaction when changing the L_g . To demonstrate the effectiveness of the proposed circuit system in producing phase locking, we conducted particle-in-cell (PIC) simulations to show that the interesting mode hopping occurs with the phase difference of 0 and π between the output signals from two output ports, corresponding to the excitation of the TM_{n1} mode with different n . Simulation results show that the oscillator can deliver two times of the output power obtained from one single oscillator at 220 GHz. The proposed scheme is promising in extending to phase locking between multiple EIOs, and generating higher power at millimeter-wave and higher frequencies. PACS codes 84.40.Fe, 07.57.Kp, 85.25.Pb

Key words: Extended interaction oscillator (EIO), distributed beam, high order mode, phase locking, vacuum electronics

PACS:

应用于亚毫米波锁相振荡器的共谐振扩展相互作用电路设计

毕亮杰^{1,2,3,4,5,6}, 李海龙^{1,2,3,4,5,6}, 王彬^{1,2,3,4,5,6}, 蒙林^{1,2,3,4,5,6}, 殷勇^{1,2,3,4,5,6}

(1. 电子科技大学, 电子科学与工程学院, 四川 成都 611731;

2. **Abstract:** 本论文提出了一种基于高阶 TM_{n1} 模的共谐振扩展相互作用电路系统方案, 用于锁定两个扩展相互作用振荡器(EIO)的相位, 以在 G 波段产生高功率。两个独立的 EIO 通过一个特定设计长度 L_g 的间隙波导内建立的单间隙耦合场耦合, 形成基于共谐振系统的锁相 EIO。作为一个整体系统, 重点研究了该系统在不同单间隙耦合场下的模式分析、模式跳变, 从而揭示了改变 L_g 时两个 EIO 注波相互作用之间相位差的变化。为了证明所提出的电路系统锁定 EIO 相位的有效性, 我们开展粒子模拟 (PIC) 研究, 表明当两个输出端口的输出信号之间的相位差为 0 和 π 时, 会发生对应于具有不同 n 的 TM_{n1} 模式的跳变。模拟结果表明, 该锁相振荡器能够在 220 GHz 下产生两倍于单个振荡器的输出功率。该方案有望扩展到多个 EIO 之间的锁相, 并在毫米波和更高频率下产生更高的功率。Key words: 扩展相互作用振荡器(EIO);

3. 分布式电子注;
4. 高阶模;
5. 锁相;
6. 真空电子学)

Introduction

EIOs are among the most powerful and compact high-frequency microwave sources in the field of vacuum electronic devices [1]. Nowadays, submillimeter wave

frequencies (100 GHz to 300 GHz) become one of the most important spectrum resources to be developed [2]. It is therefore of great interest in developing submillimeter-wave EIOs to meet the needs of high-power radiation in these frequency bands for some specific applications

Biography: BI Liang-Jie (1990-), Male, Born in Yuanping, Shanxi, China. Research interests include millimeter waves and THz vacuum electronic devices, high power microwave technique and their applications. E-mail: blj@uestc.edu.cn

* **Corresponding author:** Hailong Li, E-mail: lihailong@uestc.edu.cn; E-mail: lihailong@uestc.edu.cn

[3, 4]. However, the typical operation mechanism of conventional EIOs, each of which is driven by a single beam, requires a very small EIO circuit size due to the limitation of the operating wavelength at submillimetre-wave frequencies [5]. This limits the power level of such single-beam EIOs because a large beam current is difficult to be obtained and transported in the small circuits at a specific beam voltage. For classical EIOs, extended interaction klystrons (EIKs), and traveling wave tubes in vacuum electronics and high-power microwaves, two-beam [6]-[12], or multi-beam technology [13]-[19] associated with high order mode operation provides an effective solution for increasing beam power and accordingly increasing the output power of millimeter-wave and submillimeter-wave tubes. One typical case is to operate an EIO or an EIK with the TM_{n1} mode in the coaxial extended interaction circuit driven by multiple beams, which has been applied in Ka-band [16, 17], W-band [18], and Y-band [19]. Another case is that a type of two-beam EIO has been proposed to increase its power to kW-level at 220 GHz [20, 21]. The EIO is operated in the beam-wave interaction between two beams and a high order TM_{13} mode.

For a conventional submillimeter-wave EIO, which is driven by a single beam and has a low output power, it is of great interest to integrate two or multiple such EIOs, and then connect them together to increase the total power level from the perspective of physics mechanism and engineering. One of the most important technology is to explore efficient operation mechanism to make multiple devices operate in the same frequency and certain phase difference.

In this paper, we propose a scheme of commonly-resonated extended interaction circuits for supporting the phase locking between two G-band EIOs, which forms a high power submillimeter-wave EIO driven by two beams on the whole. The commonly-resonated extended interaction circuits are formed by using narrow gap waveguide to connect the coupling cavities of two circuits. The high order TM_{n1} mode with single-gap coupling field distributed in the gap waveguide is established to support the operation of the commonly-resonated circuit system for locking the phases of two EIOs. The resonant condition of the commonly-resonated circuit system is analyzed to show the capability of duplicating the electromagnetic characteristics of conventional single EIO circuit. Accordingly, the operation mechanism shows almost same behaviour between the two-beam circuit and one single-beam circuit of the two-beam circuit. The output power of the two-beam EIO is two times that of the conventional single-beam EIO.

It should be noted that the proposed scheme maintains excellent interaction capability between the extended interaction field and an electron beam. On this basis, such interaction capability is duplicated to form two-mirror extended interaction circuits with mutual coupling features. This scheme provides a promising solution for locking the phases of two single oscillators toward high power sub-millimeter wave radiation.

1 Design and Mode Analysis of The Commonly-Resonated Circuits for Phase Locking

The basic idea of the design derives from duplicating one typical single-beam EIO to two such identical EIOs through effective communicating them. The communication should make the two-EIO system maintain the same electromagnetic characteristics including resonant frequency, field distribution, Q factors, and interaction capability of the typical single one. For a conventional EIO, the output circuit is typically connected to one of the symmetrical coupling cavities, which consists of a coupling hole and a standard rectangular waveguide. If duplicating one identical coupling hole and connecting it to another coupling cavity, the single EIO would have two coupling ports, including 1) the typical output circuit, and 2) the coupling hole behaving for coupling signal from the EIO circuit. When another identical EIO is connected to this duplicated coupling hole, the configuration will evolve into two EIO circuits connected by one such coupling hole, as shown in Figure 1. The so-called "coupling hole" is named as gap waveguide here, because its length can be extended to behave like a waveguide for satisfying effective communications between two EIO circuits. Then two connected extended interaction circuits are formed and two output waveguide ports are symmetrically distributed on both sides of the circuit.

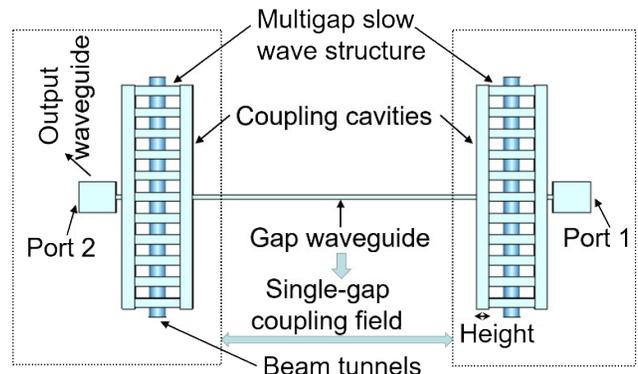


图1 基于共谐振电路系统的双电子注振荡器模型示意图

Figure 1 Schematic drawings of the models of the two-beam oscillator with the commonly-resonated circuit system.

Every extended interaction circuit consists of a multigap slow wave structure (SWS) and two symmetrical coupling cavities, as shown in Figure 1. The electron beam passes through the beam tunnel which is located across the center of the multigap SWS, and the interaction between the beam and the circuit takes place in the SWS. The period length, P , of the SWS can be calculated from the synchronous condition as following equation, $P/v_e = N/f$, where v_e is the DC velocity of the electron beam, f is the operation frequency of the circuit, N is 1 for 2π mode operation, respectively. Here, P is selected as 0.37 mm according to the designed voltage of ~ 22

kV. Through dozens of Eigenmode simulations, the gap length is determined as 0.16 mm when considering the balance between the effective characteristic impedance and the capability of the heat dissipation in the SWS. The axial length of every coupling cavity is equal to almost integral multiple (the gap number is 11 here) of a half standing wavelength. The output waveguide is WR4 standard waveguide. The two EIO circuits are designed with same geometrical parameters and connected through the gap waveguide.

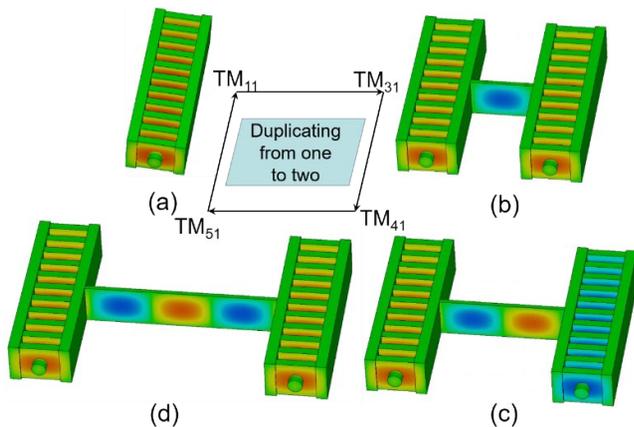


图2 典型模式纵向电场(E_z 场)的三维分布图,模式包括(a)传统单个扩展相互作用电路中 TM_{11} 模,具有不同 L_g 共振电路系统的(b) TM_{31} 模,(c) TM_{41} 模和(d) TM_{51} 模。

Figure 2 The three-dimensional pattern of the E_z field of the typical modes, including (a) the conventional TM_{11} mode in the conventional single extended interaction circuit, (b) the TM_{31} mode, (c) the TM_{41} mode, and (d) the TM_{51} mode of the commonly-resonated system with different L_g .

It is important to understand that the two connected circuits form a whole resonant system (shown in Figure 1) instead of three separate parts: two identical circuits and a gap waveguide. The operation mode of the whole system is characterized by the two identical extended interaction fields associated with the field component distributed in the gap waveguide, which behaves as three field components distributing in the cross section of the whole system. The operation mode is actually a high order TM_{n1} mode with n consisting of two extended interaction fields and $n-2$ of single-gap coupling fields in the gap waveguide. The 1 in the subscript of the TM_{n1} mode means that the E_z field of the mode of the whole system experiences one maximum value along the x direction.

It is notable that the commonly-resonated state is established, when one of the two circuits is operated with the same resonant frequency, field distribution, Q factors and beam-loading characteristics, as those of the single circuits which serves for a conventional single-beam EIO. According to the basic idea mentioned above, it is necessary to resonate the TM_{n1} mode with two respective extended interaction fields maintaining the same distribution pattern as compared with the E_z field in one of the

single-beam circuit, as shown in Figure 2(a). Figure 2(b), (c), and (d) shows the TM_{31} , TM_{41} , and TM_{51} mode respectively. These modes are characterized by two extended interaction fields with the specific single-gap coupling field. For the TM_{31} mode, the coupling field is distributed with one of half standing-wave wavelength ($\lambda_d/2$) in the gap waveguide. When the L_g is increased to be λ_d and $3\lambda_d/2$, the system is resonated in the TM_{41} and TM_{51} mode. The most important characteristics of these three modes are that the extended interaction field distributed in the both sides of extended interaction circuits maintain the same field pattern as that of the typical single circuit, as shown in Figure 2. The resonant condition of these three modes lies in the fact that the gap waveguide is resonated with the matched coupling field, because the specific L_g makes the boundaries of the gap waveguide satisfy the establishment of integer multiples of $\lambda_d/2$ even when the gap waveguide is separated with the circuits. When these boundaries are replaced with the connection between the coupling cavities and the gap waveguide, the gap waveguide would not affect the original E_z field distribution of the extended interaction circuits.

However, the L_g s corresponding to the three TM_{n1} modes are specific case for duplicating one EIO circuit to two circuits. For the general case of L_g , the E_z field across the cross section of the gap waveguide largely affects the axial distribution of the E_z field, and hence other electromagnetic characteristics. It is consequently important to analyze the effect of the length of the gap waveguide on the E_z field distribution across the cross section and frequency of the whole system. For the whole system, there exists two types of the resonated TM_{n1} modes including the mode with n of odd number and the mode with n of even number. The mode with n of odd number is characterized by making the extended interaction fields in both sides of the circuits have 0 phase. Differently, the mode with n of even number makes them have a π phase.

Figure 3 shows the effect of the L_g on the frequency of the TM_{n1} mode with n of odd number and even. Here we regard the frequency of the single extended interaction circuit as the reference point corresponding to L_g/λ of 0. When the L_g is increased, the frequency of the mode with odd number decreases firstly to the value corresponding to the point B' (First decrease), then increases sharply and thereafter decreases (Second decrease). To identify the frequency variation clearly, we set the first decrease as the stage 1, and the second decrease as the stage 2. In fact, the stage 1 corresponds to the same mode of the TM_{31} . The stage 2 corresponds to the same mode of the TM_{51} . When the TM_{31} mode is shifted to the TM_{51} mode, the frequency experiences a sharp increase. When the resonant system begins to resonate into an identical mode, its frequency is not increased as the L_g increases until the mode hopping happens.

Similarly, the frequency of the mode with n of even number experiences a decrease variation firstly, a sharp increase secondly and then a decrease thirdly. The first

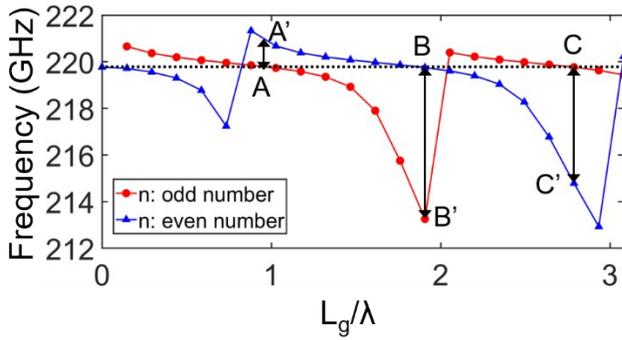


图3 L_g/λ 对 n 为奇数和偶数的 TM_{n1} 模共振系统频率的影响。

Figure 3 The effect of L_g/λ on the frequency of the resonant system associated with the resonant mode of TM_{n1} with n of odd number and even number.

decrease corresponds to the TM_{21} mode. The sharp increase corresponds to the mode hopping from the TM_{21} to the TM_{41} mode. The third decrease is because the increase of the L_g makes the field distribution of the TM_{41} mode distributed in a larger circuit structure.

It should be noted that the frequency of the TM_{n1} with n of odd number overlap that of the TM_{n1} with n of even number. When the L_g is increased in the certain range, the frequency of the TM_{31} mode is decreased from A to B'. The frequency decrease makes the frequency of the TM_{31} mode have a larger deviation from the design frequency of ~ 220 GHz. In this variation range of the L_g , the frequency of the TM_{41} mode decreases to the design value, which could replace the TM_{31} mode for supporting the system. It is therefore of great interest that the overlapping frequency between the TM_{31} and the TM_{41} mode can guide the mode selection for the effective communications of the two extended interaction circuits. Figure 3 shows the system can select the TM_{31} at the point A, the

TM_{41} at the point B, and the TM_{51} at the point C, as well as other higher order TM_{n1} mode with the specific point. These modes corresponding to the specific points are resonated in different circuit structure, however, they have the same E_z field distribution along the axis, as shown in Figure 4. So their frequencies, Q_0 factors are the same, as well as the effective interaction impedance M^2R/Q , in which M represents the coupling coefficient, and R/Q is the characteristic impedance of the interaction circuit.

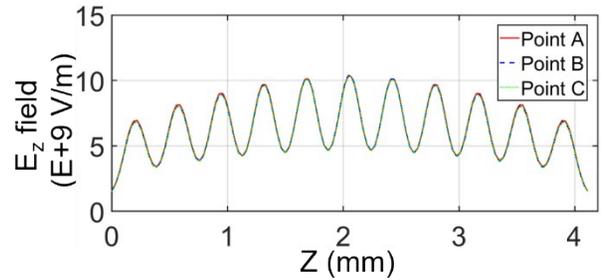


图4 图3中点A,B,C对应模式沿轴线的 E_z 场分布。

Figure 4 The E_z field distribution along the axes of the modes corresponding to A, B, C shown in Figure 3.

To select the mode for easily excitation and stable operation, we focus on the possibility of the mode competition between the mode with n of odd number and the mode with n of even number in an identical resonant system. It should be noted that there exists A and A' for the TM_{31} and TM_{41} , B and B' for the TM_{41} and TM_{31} , C and C' for the TM_{51} and TM_{41} in their respective identical system. A typical principle for mode selection is to increase the frequency separation between the operation mode and other modes. It is obvious that the frequency separation between the B and B', C and C' is much larger than that between the A and A'.

To clarify the difference between the frequency separa-

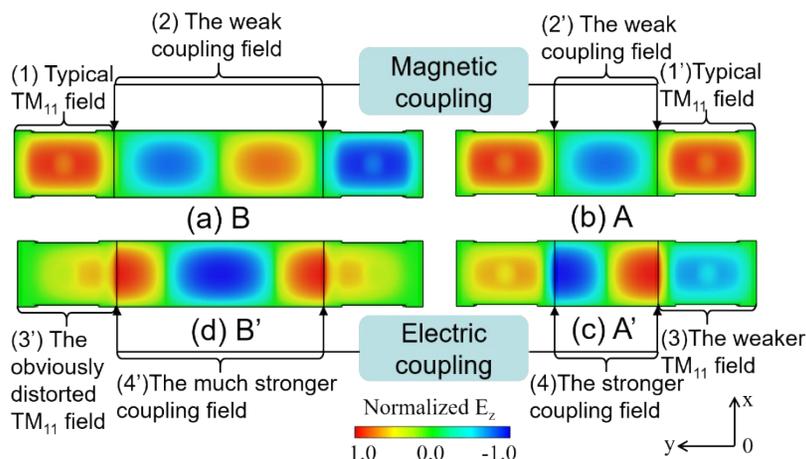


图5 点B和B'对应同一个共振系统中(a) TM_{41} 模和(d) TM_{31} 模沿横截面的 E_z 场分布。(b)和(c)分别表示点A和A'对应同一个共振系统中 TM_{31} 和 TM_{41} 模。点A和A',B和B'均为图3中标记。

Figure 5 The E_z field distribution across the cross section of (a) TM_{41} mode and (d) TM_{31} mode in the identical system corresponding to B and B', respectively. (b) and (c) shows the TM_{31} and TM_{41} mode in the identical system corresponding to A and A'. A, A', B, and B' are shown in Figure 3.

rations between A and A', B and B', we analyse the difference in E_z field distribution across the cross sections. Figure 5(b) and Figure 5(c) shows the E_z field distribution of the TM_{31} mode with the point A, and the TM_{41} mode with the point A', respectively. It is notable that the interface between the coupling cavities and the gap waveguide is characterized by two coupling types: magnetic coupling and electric coupling. For the TM_{31} mode with the point A, it is typical of magnetic coupling because the E_z field amplitude is 0 at these interfaces. However, it is electric coupling for the TM_{41} mode with the point A' because the E_z field amplitude is not 0. This compresses the space of the extended interaction circuits on one side of the system, where the E_z field is distributed. The frequency is therefore increased to be larger than that of the TM_{31} mode with the point A.

For every extended interaction circuit, the typical TM_{11} field is established in the circuit, which support the desired resonant frequency. Then an effective connection between two such extended interaction circuits is to maintain the typical TM_{11} field distribution in the circuit after connecting them by designing a proper gap waveguide. To explain the effect of the E_z field distribution on the frequency separations between A, A', and B, B', we regard the field in part (1) and (1') as the typical TM_{11} field distributed across the cross section, as shown in Figure 5(a) and (b), respectively. The frequency of point A and B is same because the distribution pattern of the typical TM_{11} field is same in the part (1) and (1'), which reproduces the typical field in the individual extended interaction circuit. This lies in the fact that the coupling field across the gap waveguide is weaker than the typical TM_{11} field, and more importantly, the coupling field is resonated with the magnetic coupling at the interfaces between the circuit and the gap waveguide, as shown in the weak field (2) and (2'), respectively.

The typical TM_{11} field in (1') is significantly weakened and become the weaker field in (3) when the field distribution of the point A is compared with that of the point A', as shown in Figure 5(c). The weak coupling field in (2') turns into the stronger coupling field in (4). It should be noted that the weak field in (3) still maintains the basic distribution pattern of the typical TM_{11} field, although the field strength of the former is smaller than that of the latter. The frequency separation between A and A' is consequently not large.

Differently for the TM_{41} mode with the point B, and the TM_{31} mode with the point B', as shown in Figure 5(a) and (d) respectively, the typical TM_{11} field in (1) is transferred into the obviously distorted TM_{11} field in (3'). The 'distorted field' is defined here because the field in (3') does not maintain the basic distribution pattern of the typical TM_{11} field, as well as the weak field in (3). The distortion of the basic distribution pattern results in a larger frequency separation between B and B', in contrast to the frequency separation between A and A'. In addition, the weak field in (2) is transferred into the much stronger coupling field in (4'). The strong field is mostly distributed in the part (1) for the point B,

however, in the part (4') for the point B'. The cross section of the part (1) is smaller than that of the part (4'). This means the strong field is mostly distributed along a larger cross section for the point B'. The frequency of the point B' is consequently smaller than that of the point B.

In fact, the comparison between the modes with the point A, A', and B, B' follows the following principles, a) the distribution pattern and the distributed space of the stronger field of the TM_{n1} mode mostly determines the frequency of the connected circuit, and b) the degree of the distortion of the typical TM_{11} field (in the individual extended interaction circuit) determines the frequency interval between the TM_{n1} modes. Based on a), the strongest field of the TM_{31} mode with the point B' is distributed across the gap waveguide, which makes the typical TM_{11} field (in part (1)) in the individual circuit on both sides of this gap waveguide be distorted severely. However, the typical TM_{11} field pattern is basically maintained in the individual circuit for the mode with the point A', as compared with the field pattern in the part (1) and (1'). It is accordingly deduced from the comparison between the E_z field distributions of the B, B' and A, A' that the frequency interval between B and B' is larger than that between A and A'.

From the perspective of the coupling condition between the coupling cavities and the gap waveguide, the magnetic coupling is distributed at the interfaces between the coupling cavities and the gap waveguide for the point B. For the point B', however, strong electric couplings occur at these interfaces, which makes the E_z field distribution in the extended interaction circuits become more distorted. It is consequently reasonable that the frequency separation between the B and B' is much larger than that between the A and A'.

2 PIC Simulations

To show the effectiveness of the two-beam oscillator in improving the output power to two times the power of the single-beam oscillator, we firstly conducted the PIC simulations [22] of the single-beam oscillator driven by the electron beam with current of the 0.6 A and voltage of 23 kV. The constant magnetic field of 1 T is used to confine the beam transportation in the beam tunnel. Figure 6(a) shows that the conventional single-beam oscillator can deliver ~1.65 kW at ~220 GHz. The corresponding phase space of the electron beam is shown in Figure 6(b), which indicates that an effective beam-wave interaction takes place in the single-beam oscillator.

To examine the operation capability of the proposed resonant system, we designed two symmetrical output circuits consisting of two identical coupling holes and standard rectangular waveguides, to form the two-beam oscillator. It is notable that the output circuit on one side of the resonant system is the same as the output circuit of the single-beam oscillator. The PIC simulations are used to calculate the interaction between two beams and the circuit system. Two beams with voltage of 23 kV and each current of 0.6 A are injected into the two beam tun-

nels for driving the oscillator. The constant magnetic field of 1 T is also used to confine the two electron beams.

The important task is to calculate the effect of the L_g on the output performance of the oscillator when the two beams are loading into the oscillator. Figure 7 shows the corresponding PIC simulation results as the L_g is increased. It is of great interest that the output power of the oscillator is increased firstly (the first increase), decreased secondly and then increased (the second increase), decreased thirdly and then increased (the third increase). The frequencies of the variation stages with the first, second, and third increase are all decreased. However, there is a frequency jump between the first and second increase, as well as the second and third increase. The frequency jump shows the mode hopping between each stage of the increase. The first, second, third increase corresponds to the operation of the TM_{31} , TM_{41} , and TM_{51} mode through analyzing the electron trajectory and the E_z field distribution of each stage. It is shown as a result of the resonant frequencies of the system (Figure 3) that the TM_{31} , TM_{41} , and TM_{51} mode can be efficiently excited when the frequency of the system is close to the resonant frequency of these modes respectively. This is because the synchronous conditions of these modes are satisfied, respectively.

To clarify the operation modes of the three increases, we present the output signals, phase spaces, electron trajectories corresponding to three typical L_g s in the

three respective stages. Figure 8 shows that the output signals of the two waveguide ports have the same phase, which can be verified from the phase spaces and electron trajectories. This demonstrates the two-beam oscillator with L_{g1} is operated with the TM_{31} - 2π mode. Figure 8(a) shows the output power from each port is ~ 1.65 kW, which is almost the same as the output power of one single EIO, as shown in Figure 6(a). The total power of the two-beam oscillator is ~ 3.3 kW. The frequencies of two output waves from two ports are consistent of 220.2 GHz. This lies in the fact that the two extended circuits are formed to be a whole resonant system although it has two output ports.

Figure 9 shows the simulation results of the oscillator with L_{g2} when it is operated with the TM_{41} - 2π mode. Figure 9(a) shows the output powers from two ports are the same and the total power is ~ 3.2 kW. The phase difference between two output signals from two ports is π , as shown in Figure 9(b). The frequency is 220.3 GHz. The electron trajectories show the two beams of electrons move with π phase, as shown in Figure 9(d).

When the ohmic loss is considered at G-band, the PIC simulations are conducted with the electric conductivity of $2.2e7$ S/m [23]-[26]. The simulation results show that the output signals from two ports still have a certain phase difference when the L_g is different. The total output power of ~ 1 kW can be obtained with the same frequency of ~ 220 GHz.

图 11 当耦合桥长为 L_{g2} 的锁相振荡器被电压 23

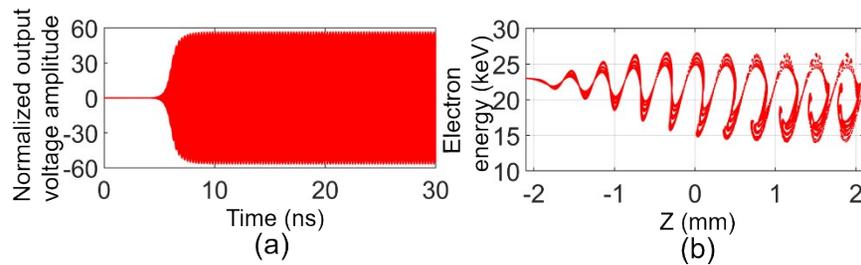


图 6 当电压 23 kV 电流 0.6 A 的电子注驱动基于共振系统中单个扩展相互作用电路的传统单个 EIO 时, 该图表示 (a) 单个端口的输出信号和 (b) 电子的相空间图。

Figure 6 When the conventional single EIO based on one of the extended interaction circuit in the commonly-resonated circuits is driven by an electron beam with the current of 0.6 A at 23 kV, this figure shows (a) the output signal from the single port, and (b) the phase space of the electrons.

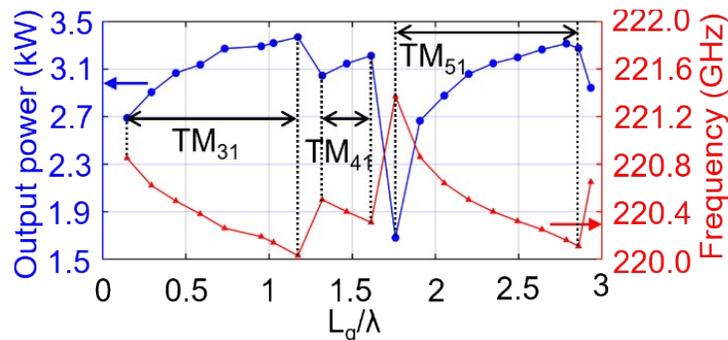


图 7 L_g/λ 对所提出的锁相振荡器输出功率和频率的影响。

Figure 7 The effect of the L_g/λ on the output power and frequency of the proposed phase-locked oscillator.

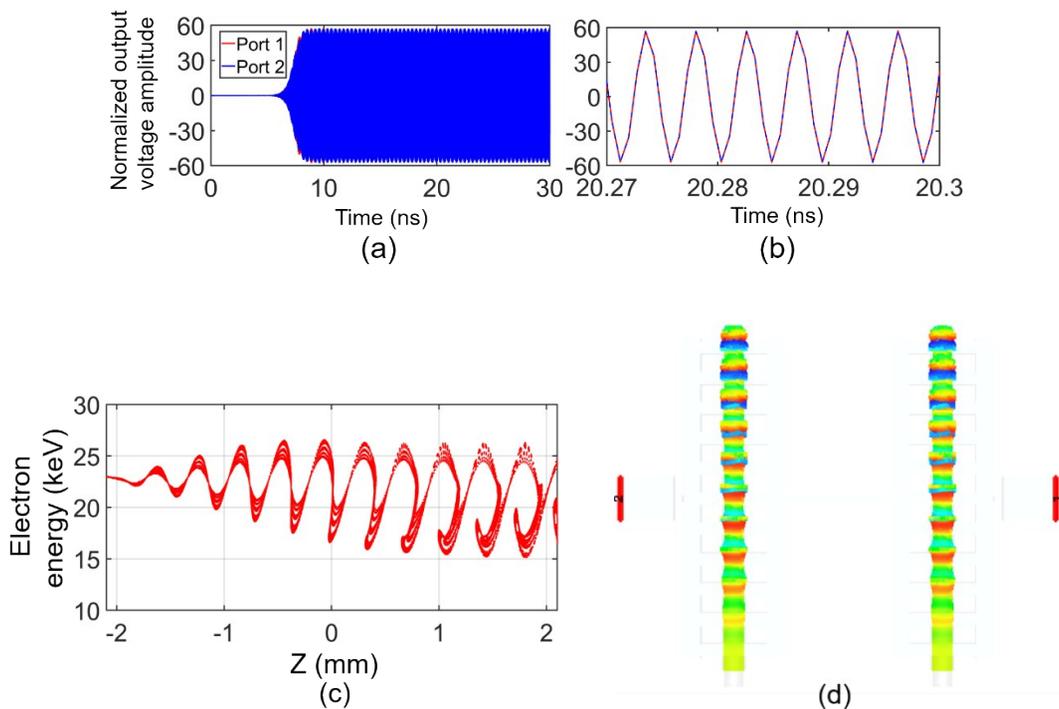


图8 当耦合桥长为 L_{g1} 的锁相振荡器被电压23kV下具有相同注电流0.6A的双电子注驱动时,该图表示(a)两个端口的输出信号,(b)用于显示相位差的20.27ns到20.3ns之间信号的详细信息,(c)双注电子的相空间图和(d)双注电子的轨迹。

Figure 8 When the oscillator with L_{g1} is driven by two beams with the same current of 0.6 A at 23 kV, this figure shows (a) the output signals from two ports, (b) the detailed information of the signal from 20.27 ns to 20.3 ns showing the phase difference, (c) the phase space of the two beams of electrons, and (d) the electron trajectories.

kV下具有相同注电流 $I_1=I_2$ 的双电子注驱动时,该图表示当 $I_1(I_2)$ 从0.2 A增大到1 A时该振荡器的输出功率变化规律。

Figure 10 shows the pic simulation results of the oscillator with L_{g3} when it is operated with the $TM_{51-2\pi}$ mode. Figure 9 (a) shows the output powers from two ports are the same and the total power is ~ 3.2 kW. The phase difference between two output signals from two ports is 0, as shown in Figure 10(b). The frequency is ~ 220.3 GHz. The electron trajectories show the two beams of electrons move with 0 phase, as shown in Figure 10(d).

The two beams are expected to be generated by two separate cathodes. In the PIC simulations, the radius of the electron beam is 0.12 mm, and the radius of the beam tunnel is 0.15 mm. Figure 11 shows the electron beam with relatively small current, for example, 0.2 A, 0.3 A would be appropriate to use mechanism of thermionic cathodes to generate. For higher power specification, larger current is required for driving the oscillator. However, the electron beam with large current, for example, 0.6 A and above, is difficult to be generated using thermionic cathodes. It is reasonable to use pseudospark discharging system [27, 28] to generate the electron beam with large current density (1326 A/cm² corresponding to the current of 0.6 A).

For the two beams, it is reasonable to predict that

the two beam currents may be different at a specific voltage in practice. To examine the oscillator performance with two different beam parameters, we used PIC simulations to calculate the effect of two different beam currents on the performance at the beam voltage of 23 kV. Figure 12 shows the output power of the oscillator driven by one beam with the current of I_2 and another beam with the current of I_1 . Here I_1 is assumed to be constant of 0.6 A, and I_2 is assumed to be increased from 0.2 A to 0.6 A. Correspondingly, the output power is increased from 2.1 kW to 3.2 kW. The frequency is almost not changed because the oscillator is operated with the same mode TM_{41} . When the two beam currents are 0.6 A and 0.4 A, the output powers generated from two output ports have a slight difference, as shown in Figure 13(a). Accordingly, the phase difference of the signals from two ports is π , as shown in Figure 13(b).

Figure 14 shows the variations of the output power and frequency versus different waveguide lengths for one beam current of 0.6 A and another current of 0.4 A. When the length of the coupling waveguide (L_g) is increased, the frequency is firstly decreased, then increased sharply and starts to decrease until next increasing. For every stage of the frequency decreasing, the output power is increased and the phase-locked oscillator is operated in the same mode. Every sharp increase in the frequency corresponds to the mode hopping in the oscilla-

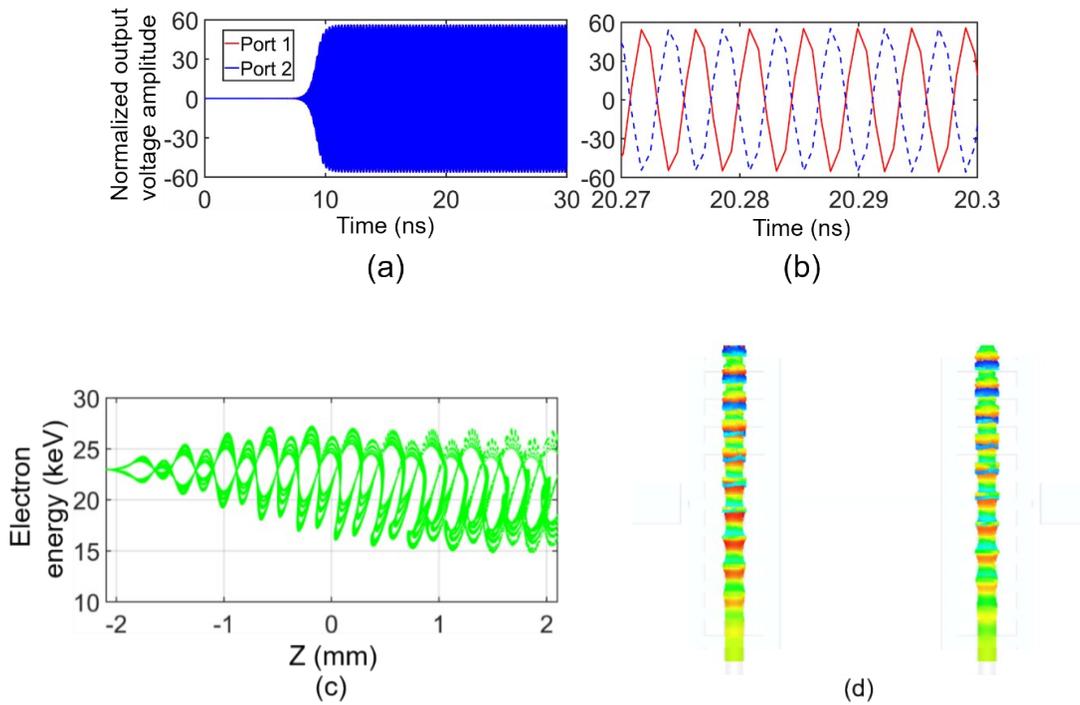


图9 当耦合桥长为 L_{g_2} 的锁相振荡器被电压23 kV下具有相同注电流0.6 A的双电子注驱动时,该图表示(a)两个端口的输出信号,(b)用于显示相位差的20.27 ns到20.3 ns之间信号的详细信息,(c)双注电子的相空间图和(d)双注电子的轨迹。

Figure 9 When the oscillator with L_{g_2} is driven by two beams with the same current of 0.6 A at 23 kV, this figure shows (a) the output signals from two ports, (b) the detailed information of the signal from 20.27 ns to 20.3 ns showing the phase difference, (c) the phase space of the two beams of electrons, and (d) the electron trajectories.

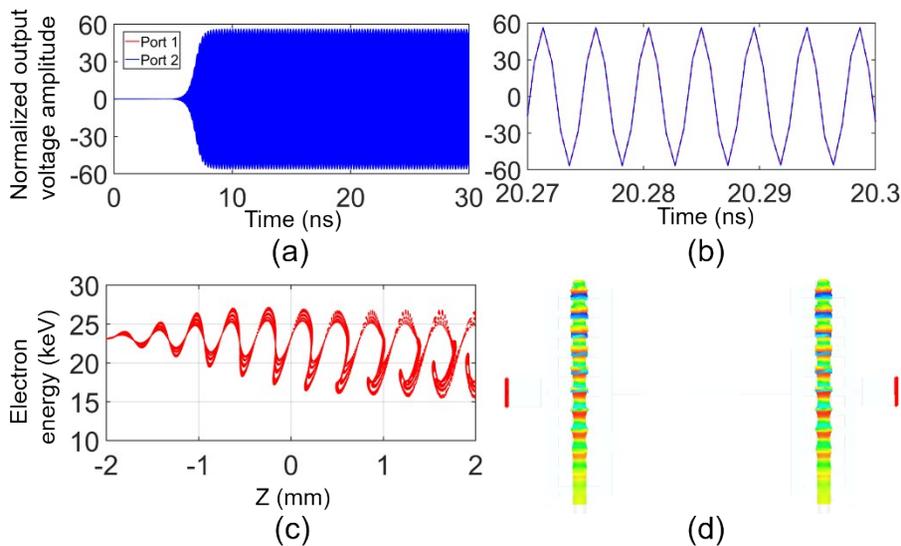


图10 当耦合桥长为 L_{g_3} 的锁相振荡器被电压23 kV下具有相同注电流0.6 A的双电子注驱动时,该图表示(a)两个端口的输出信号,(b)用于显示相位差的20.27 ns到20.3 ns之间信号的详细信息,(c)双注电子的相空间图和(d)双注电子的轨迹。

Figure 10 When the oscillator with L_{g_3} is driven by two beams with the same current of 0.6 A at 23 kV, this figure shows (a) the output signals from two ports, (b) the detailed information of the signal from 20.27 ns to 20.3 ns showing the phase difference, (c) the phase space of the two beams of electrons, and (d) the electron trajectories.

tor and at this operating point, the output power is decreased sharply. The operating mode is shifted from the

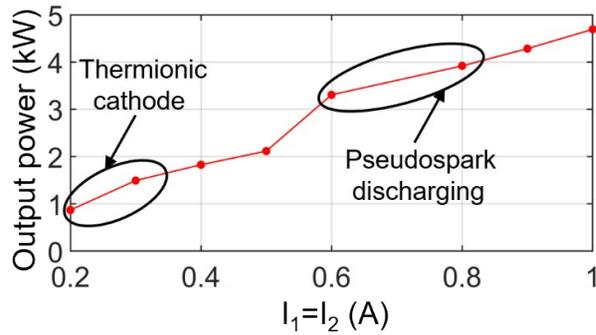


Figure 11 When the oscillator with L_{g2} is driven by two beams with the same current of $I_1=I_2$ at 23 kV, this figure shows the output power of the two-beam oscillator as increasing the I_1 (I_2) from 0.2 A to 1 A.

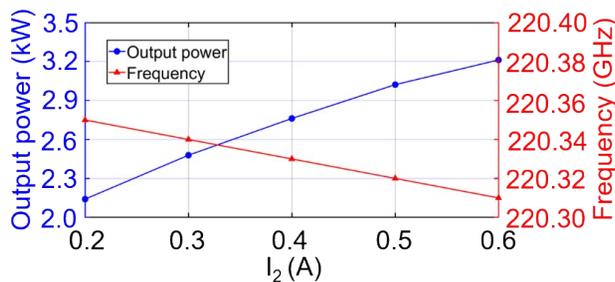


图 12 当双注中一个电子注电流 I_1 为 0.6 A 且另一个电流 I_2 从 0.2 A 增大到 0.6 A 时, 该振荡器的输出功率和频率。

Figure 12 The output power and frequency of the oscillator driven by the two beams with one current I_1 of 0.6 A and another current I_2 increasing from 0.2 A to 0.6 A.

TM_{31} , TM_{41} , to TM_{51} mode as the L_g is increased within the full range, as shown in Figure 14.

For the design scheme of the phase-locked oscillator, the coupling waveguide is located between the two coupling cavities of the two EIO cavities. The matching between the coupling waveguide and two coupling cavities is therefore important to lock the phases of the two EIOs. Then we focus on the effect of the height errors of

the coupling cavities of one EIO cavity on the phase-locking performance. The height of the coupling cavities is shown in Fig. 1 and the height error is defined as the variation relative to the original height of the coupling cavities of one EIO cavity. The dimensions of another EIO are unchanged. The EIO cavity can be fabricated by using the micro-CNC, which can provide a fabricating tolerance of $\pm 2 \mu\text{m}$ [29]. Figure 15 shows that when the height error is increased within $\pm 8 \mu\text{m}$, the total output power from two ports is firstly increased corresponding to the error within $-8 \mu\text{m}$ and 0, and secondly decreased corresponding to the error within 0 and $8 \mu\text{m}$. The maximum and minimum power is 3.1 kW and 2.8 kW, respectively. The frequencies of the output signals from two ports are uniform. It is within 220.4 GHz and 220.56 GHz, which is almost unchanged. This indicates that the height error could satisfy the fabrication accuracy of the CNC.

To present the effect of the height error on the phases of the output signals from two ports, we show the pic simulation results of the phase-locked oscillator with the height error of $2 \mu\text{m}$, as shown in Figure 16. Figure 16 (a) shows that the amplitude of the output signals from two ports have a difference due to the introduction of the height error, which brings the frequency difference between two EIO cavities with free-running state. The designed proper coupling waveguide makes the two EIO cavities being locked to produce a single frequency, which means that the commonly-resonated EIO is operated in a single mode (TM_{31} mode). Figure 16 (b) shows that the phase difference between the two output signals is almost 0. The oscillator with the height error within the full range shown in Figure 15 can still be operated in the same single mode and produce in-phase signals.

3 Conclusion

In this paper, a novel scheme and its specific operation mechanism for a G-band two-beam EIO with two output ports has been proposed with locking the phases of two extended interaction circuits through a specifically designed gap waveguide, which is conceived to generate

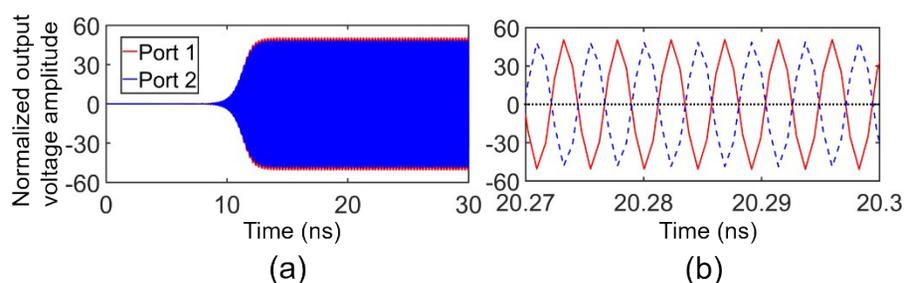


图 13 当耦合桥长为 L_{g2} 的振荡器被电压 23 kV 下一个电流为 0.6 A 且另一个电流为 0.4 A 的双电子注驱动时, 该图表示 (a) 两个端口的输出信号和 (b) 用于显示相位差的 20.27 ns 到 20.3 ns 之间信号的详细信息。

Figure 13 When the oscillator with L_{g2} is driven by two beams with the one current of 0.6 A and another current of 0.4 A at 23 kV, this figure shows (a) the output signals from two ports and (b) the detailed information of the signal from 20.27 ns to 20.3 ns showing the phase difference.

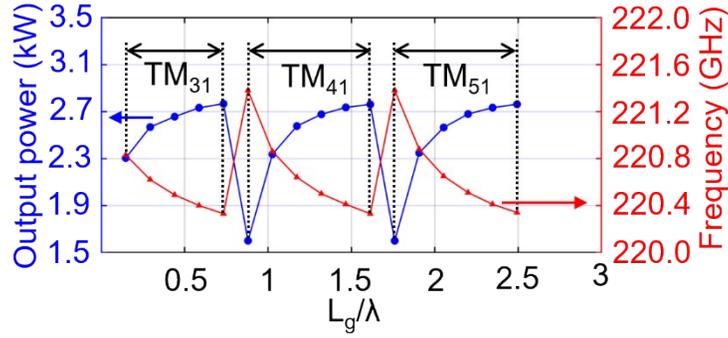


图 14 当所提出的锁相振荡器被一个电流为 0.6 A 且另一个电流为 0.4 A 的双电子注驱动时, L_g/λ 对振荡器输出功率和频率的影响。

Figure 14 The effect of the L_g/λ on the output power and frequency of the proposed phase-locked oscillator with one beam current of 0.6 A and another beam current of 0.4 A.

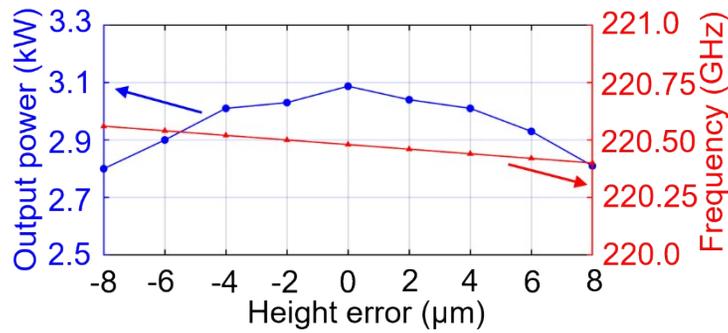


图 15 当锁相振荡器被双注电流均为 0.6 A 的双电子注驱动时, 其中一个 EIO 腔体的耦合腔高度容差 (另一个 EIO 腔体耦合腔尺寸不变) 对振荡器输出功率和频率的影响。

Figure 15 The effect of the height error of the coupling cavities of one EIO cavity (with the coupling cavities of another EIO cavity unchanged) on the power and frequency of the phase-locked oscillator (the two beam currents are assumed to be same of 0.6 A).

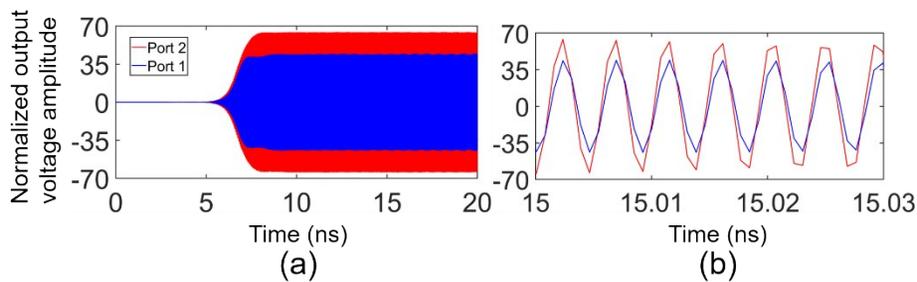


图 16 当高度容差为 2 μm 时, 被两个注电流均为 0.6 A 双电子注驱动的锁相振荡器能够产生的 (a) 两个端口输出信号和 (b) 用于显示相位差的 15 ns 到 15.03 ns 之间信号的详细信息。

Figure 16 When the height error is 2 μm , the oscillator (with two beam currents of 0.6 A) can produce (a) the output signals from two ports and (b) the detailed information of the signal from 15 ns to 15.03 ns showing the phase difference.

high power submillimeter-wave radiation. The commonly-resonated circuit system is therefore formed and the high order TM_{n1} modes with specific single-gap coupling fields is established to support the commonly-resonated condition of the system and phase locking between two EIOs. The mode analysis with different n and mode hopping has been analysed to support the mode selection for the two-beam oscillator.

Accordingly, the mode hopping occurs between spe-

cific TM_{n1} modes with different n when the oscillator designed with the gap waveguide having different length, is driven by two electron beams. PIC simulation results show that the proposed oscillator can be shifted by exciting the TM_{n1} mode with different n to deliver two signals with phase difference of 0 and π from two output ports. Consequently, the oscillator can reproduce the interaction capability of one of the conventional single-beam oscillator and produce higher power, which is two times the

power of the single oscillator. When the two beams have different currents, the oscillator can still show efficient interaction with phase difference of 0 or π for the two beams. It is of great interest that the proposed scheme can be operated in the TM_n mode with a large n to support the phase locking between two EIOs. This is promising in applications of powerful, compact and efficient sub-millimetre wave and higher frequency vacuum electronic devices.

Acknowledgment

This work was supported in part by National Natural Science Foundation of China (No. 62401125), Natural Science Foundation of Sichuan Province (No. 2023NSF-SC1376), and Fundamental Research Funds for the Central Universities (No. ZYGX2024J008).

References

- [1] J. H. Booske, R. J. Dobbs, C. D. Joye, C. L. Kory, G. R. Neil, G. S. Park, J. Park, and R. J. Temkin, Vacuum electronic high power Terahertz sources, *IEEE Trans. Terahertz Science and Technology*, 1, 1 (2011).
- [2] S. S. Dhillon, M. S. Vitiello, E. H. Linfield, A. G. Davies, M. C. Hoffmann, J. Booske, C. Paoloni, M. Gensch, P. Weightman, G. P. Williams, E. C. Camus, D. R. S. Cumming, F. Simoens, I. E. Caranza, J. Grant, S. Lucyszyn, M. K. Gonokami, K. Konishi, M. Koch, C. A. Schmuttenmaer, T. L. Cocker, R. Huber, A. G. Markelz, Z. D. Taylor, V. P. Wallace, J. A. Zeitler, J. Sibik, T. M. Korter, B. Ellison, S. Rea, P. Goldsmith, K. B. Cooper, R. Appleby, D. Pardo, P. G. Huggard, V. Krozer, H. Shams, M. Fice, C. Renaud, A. Seeds, A. Stohr, M. Naftaly, N. Ridler, R. Clarke, J. E. Cunningham, and M. B. Johnston, The 2017 Terahertz science and technology roadmap, *Journal of Physics D: Applied Physics*, 50, 4 (2017).
- [3] J. H. Booske, Plasma physics and related challenges of millimeter-wave-to-terahertz and high power microwave generation, *Phys. Plasmas*, 5, 16 (2008).
- [4] B. Steer, A. Roitman, P. Horoyski, M. Hyttinen, R. Dobbs, D. Berry, "Millimeter-wave extended interaction klystrons for high power ground, airborne and space radars," in *Proceedings of 41st European Microwave Conference*, (Manchester, United Kingdom, 2011), pp. 984–987.
- [5] D. Berry, H. Deng, R. Dobbs, P. Horoyski, M. Hyttinen, A. Kingsmill, R. MacHattie, A. Roitman, E. Sokol, and B. Steer, "Practical aspects of EIK technology," *IEEE Trans. Electron Devices*, 61, 6 (2014).
- [6] K. Li, W. Liu, Y. Wang, M. Cao, and S. Liao, Enhancement of the output power of terahertz folded waveguide oscillator by two parallel electron beams, *Phys. Plasmas*, 22, 11 (2015).
- [7] W. Liu, K. Li, P. Gao, C. Zhao, X. Guo, and Z. Zhang, Nonlinear theory for beam-wave interactions of two electron beams with higher order TE₂₀ mode in serpentine waveguide traveling wave amplifier, *Phys. Plasmas*, 25, 12 (2018).
- [8] H. Wang, Q. Xue, D. Zhao, Z. Qu, and H. Ding, A wideband double-sheet-beam extended interaction klystron with ridge-loaded structure, *IEEE Trans. Plasma Science*, 39, 3 (2011).
- [9] C. Xu, L. Meng, C. Hu, Y. Yin, S. Zhu, Z. Chang, L. Bi, R. Peng, B. Wang, H. Li, and X. Yuan, Analysis of dual-frequency radiation from a G-band extended interaction oscillator with double sheet electron beam, *IEEE Trans. Electron Devices*, 66, 7 (2019).
- [10] Y. Gong, H. Yin, L. Yue, Z. Lu, Y. Wei, J. Feng, Z. Duan, and X. Xu, A 140-GHz two-beam overmoded foled-waveguide traveling-wave tube, *IEEE Trans. Plasma Science*, 39, 3 (2011).
- [11] Y. Tian, G. Shu, Y. Gong, W. He, A novel slow-wave structure-coupled double folded waveguide operating at high-order TM₂₀ mode for Terahertz TWT, *IEEE Electron Device Letters*, 42, 12 (2021).
- [12] L. Bi, Y. Qin, C. Xu, R. Peng, L. Meng, B. Wang, H. Li, and Y. Yin, Design and analysis of an overmoded circuit for two-beam sub-THz extended interaction oscillator, *IEEE Trans. Electron Devices*, 68, 11 (2021).
- [13] S. Li, H. Huang, Z. Duan, B. N. Basu, Z. Liu, H. He, Z. Wang, Demonstration of a Ka-band oversized coaxial multi-beam relativistic klystron amplifier for high power millimeter-wave radiation, *IEEE Electron Device Letters*, 43, 1 (2022).
- [14] L. Sun, H. Huang, S. Li, Z. Liu, H. He, Q. Xiang, K. He, X. Fang, Investigation on high-efficiency beam-wave interaction for coaxial multi-beam relativistic klystron amplifier, *Electronics*, 11, 2 (2022).
- [15] S. Lv, C. Zhang, S. Wang, Y. Wang, Stability analysis of a planar multiple-beam circuit for W-band high power extended interaction klystron, *IEEE Trans. Electron Devices*, 62, 9 (2015).
- [16] X. Zhang, R. Zhang, and Y. Wang, Research on a high-order mode multibeam extended interaction oscillator with coaxial structure, *IEEE Trans. Plasma Science*, 48, 6 (2020).
- [17] Y. Yin, F. Zeng, B. Wang, H. Li, L. Bi, Z. Chang, R. Peng, S. Zhu, C. Xu, and L. Meng, Preliminary study of a multiple-beam extended interaction oscillator with coaxial structure, *IEEE Trans. Electron Devices*, 65, 6 (2018).
- [18] Y. Yin, L. Bi, B. Wang, P. Zhang, H. Li, W. Li, F. Zeng, R. Peng, S. Zhu, C. Xu, Z. Chang, and L. Meng, Preliminary circuit analysis of a W-band high power extended interaction oscillator with distributed hollow electron beam, *IEEE Trans. Electron Devices*, 66, 7 (2019).
- [19] F. Lin, S. Wu, Y. Xiao, and L. Zhang, A 0.3 THz multi-beam extended interaction klystron based on TM_{10,10} mode coaxial coupled cavity, *IEEE Access*, 8, 12 (2020).
- [20] L. Bi, Y. Yin, B. Wang, H. Li, R. Peng, C. Xu, Y. Qin, and L. Meng, Tractable resonant circuit with two nonuniform beams for a high-power 0.22-THz extended interaction oscillator, *IEEE Electron Device Letters*, vol. 42, 6 (2021).
- [21] L. Bi, X. Jiang, Y. Qin, C. Xu, B. Wang, Y. Yin, H. Li, and L. Meng, Power enhancement of sub-Terahertz extended interaction oscillator based on overmoded multi-gap circuit and linearly distributed two electron beams, *IEEE Transactions on Electron Devices*, 69, 2 (2022).
- [22] "CST-Computer Simulation Technology", <https://www.cst.com/Products/csts2> (March 10, 2017)
- [23] M. P. Kirley, and J. H. Booske, Terahertz conductivity of copper surfaces, *IEEE Trans. Terahertz Science and Technology*, 5, 6 (2015).
- [24] P. Pan, Y. Tang, X. Bian, L. Zhang, Q. Lu, Y. Li, Y. Feng, J. Feng, A G-band traveling wave tube with 20 W continuous wave output power, *IEEE Electron Device Letters*, 41, 12 (2020).
- [25] R. Li, C. Ruan, H. Zhang, T. U. Haq, Y. He, S. Shan, Theoretical design and numerical simulation of beam-wave interaction for G-band unequal-length slots EIK with rectangular electron beam, *IEEE Trans. Electron Devices*, 65, 8 (2018).
- [26] C. Zhang, S. Lv, J. Cai, P. Pan, and J. Feng, Exploration of a kilowatt-level Terahertz amplifier based on higher-order mode interaction, *IEEE Trans. Electron Devices*, 69, 9 (2022).
- [27] G. Shu, L. Zhang, H. Yin, J. Zhao, A. D. R. Phelps, A. W. Cross, G. Liu, Y. Luo, Z. Qian, and W. He, Experimental demonstration of a Terahertz extended interaction oscillator driven by a pseudospark-sourced sheet electron beam, *Applied Physics Letters*, vol. 112, 3 (2018).
- [28] L. Zhang, A. D. R. Phelps, K. Ronald, and A. W. Cross, Simulations of the self-focused pseudospark-sourced electron beam in a background ion channel, *IEEE Access*, 9, 11 (2022).
- [29] J. Liao, G. Shu, G. Lin, J. Lin, Q. Li, J. He, J. Ren, Z. Chang, B. Xu, J. Deng, G. Liu, C. Ruan, and W. He, Study of a 0.3-THz extended interaction oscillator based on the pseudospark-sourced sheet electron beam, *IEEE Transactions on Plasma Science*, 51, 8 (2023).